Evaluating a 3D Ultrasound Imaging Resolution of Single Transmitter/Receiver with Coding Mask by Extracting Phase Information

Mohammad Syaryadhi , Eiko Nakazawa , Norio Tagawa * , Ming Yang

Posted Date: 7 December 2023

doi: 10.20944/preprints202312.0532.v1

Keywords: single transducer; coding mask; frequency subband compound; SCM

Article

Evaluating a 3D Ultrasound Imaging Resolution of Single Transmitter/Receiver with Coding Mask by Extracting Phase Information

Mohammad Syaryadhi *, Eiko Nakazawa, Norio Tagawa and Ming Yang

Graduate School of Systems Design, Tokyo Metropolitan University, Asahigaoka 6-6, Hino, 191-0065 Tokyo, Japan; syaryadhi-mohd@ed.tmu.ac.jp (M.S.); nakazawa-eiko@ed.tmu.ac.jp (E.N.); tagawa@tmu.ac.jp (N.T.); yang@tmu.ac.jp (M.Y.)

* Correspondence: syaryadhi-mohd@ed.tmu.ac.jp

Abstract: We are currently investigating the ultrasound imaging of a sensor consisting of a randomized encoding mask attached to a single lead zirconate titanate (PZT) oscillator for use in a puncture microscope. The proposed model was performed using a finite element method (FEM) simulator. To increase the number of measurements required by a single element system, the transducer was rotated at different angles. The image was constructed by solving a linear equation of the image model. In a previous study, the image resolution was improved by extracting phase information. In this study, we propose a strategy by integrating the weighted frequency subbands compound and a super resolution method (SCM) to improve the resolution in range and lateral resolution. We also evaluated the image performance by applying different methods to improve the image quality. The results show that better image resolution and speckle suppression were obtained by applying the proposed method.

Keywords: single transducer; coding mask; frequency subband compound; SCM

1. Introduction

Ultrasound imaging has been widely applied to medical diagnosis due to its superiority such as non-ionizing radiation and relatively low-cost system. At present, it is carried out by using an array system, which requires a number of sensors arranged properly and applies a general beamforming method. For accurate diagnosis, it should have high resolution and high signal to noise ratio (SNR), and therefore researchers have intensively studied many methods to have a better image quality [1–10].

In the current pathological examination the tissue diagnosis takes a certain time for its performance. It is started by obtaining the tissue sample of human body by biopsy process that gives a burden to the patient and performs the observation under a standard optical microscope. It can be solved by developing an ultrasonic puncture microscopy which is possible to capture the tissue area of human body directly with easy in operation and comfortable to the patient. However, such device should have a simple compact structure system and not suitable implemented by a sensor array due to a huge wiring and complex electronic circuit for generating the ultrasound image [11–16].

Recently, structured ultrasound microscopy (SUM) has been proposed by using a single transmitter/receiver circuit [17,18]. However, single transducers with a single time-series echo signal required several additional measurements compared to array transducers consisting of numerous elements to construct a 3D image. Therefore, it was integrated by attaching an acoustic mask with irregular abberations to establish spatial coding. Randomizing the thickness of the coding mask affects to different delay time of the transmission signal traveling inside the mask and finally releases a randomized wave propagation in the target medium. The reflection signals from the scatterers with different delays are also received by the same transducer in a single accumulated echo signal. By rotating the transducer, variation of measurements have been obtained for enlarging the spatial coding variation of the region of interest (ROI).

Preprints (www.preprints.org) | NOT PEER-REVIEWED | Posted: 7 December 2023 doi:10.20944/preprints202312.0532.v1

Currently, we have developed techniques for improving the ultrasound image resolution based on array transducer [19–22]. Nevertheless, we are also studying the methods to improve the image quality of single element system that not explored widely yet. Our initial researches related to single transducer ultrasound imaging were reported in [23,24] by implementing a weighted frequency subbands compounding to obtain the better image resolution in range direction. We also introduced super-resolution correlation method (SCM) to single transducer [25,26]. The primary contribution of this study can be listed clearly as follows:

- to develop ultrasound imaging based on single element,
- to apply the frequency subband compound and SCM methods for improving image resolution based on the proposed model, and
- to evaluate the image performance by applying several method,
- to integrate the frequancy subbands compound and super-resolution method (SCM) to obtain a better image quality.

2. Methods

2.1. Image model

In this study, the measured data in radio frequency (RF) signal form was converted into in-phase quadrature (IQ) signal for baseband processing. The image model was constructed using the following model

$$y = Dx, \tag{1}$$

where y is a vector that consists of the time sampling series of the measured IQ echo signal, and M-column vectors of matrix D are the time sampling series of the IQ reflectance signals from each grid in the region of interest (ROI) of the imaging area. D is assumed to be known a priori. The vector x consists of the complex reflection coefficients corresponding to each grid and is obtained by solving numerically the image model.

2.2. Proposed method: integrating weighted frequency subbands compound and super-resolution method (SCM)

Many researchers have been studied the methods for improving the ultrasound imaging based on sensor array system. In previous study, we studied the weighted frequency subbands compound and super-resolution methods (SCM) for improved the image resolution based on single element instead of array system. In this study, both methods were integrated to be proposed to enhance the image quality as shown in Figure 1.

In this method, the wighted frequency subbands compound and super-resolution method (SCM) was conducted separately. We define the measurement data at M-different angles of rotation by $y = [y_1, y_2, ..., y_M]$ and $D = [D_1, D_2, ..., D_M]$. The wide base-band of the measured signal was separated into N narrow-subbands and M-angle of rotations. After applying I-Q detector, solution-x was computed numerically for each subabands and angle of rotations resulting $M \times N$-images (tensor data X). The weighted frequency subband compound was applied to the second-order tensor data X by following mean-variance distortion-free response (MVDR) method. Detail of MVDR can be seen clearly in Appendix-A. The method is started by determining the variance-covariance matrix (R) from snapshot vector-$p_i(t)$. In array system, the variance covariance matrix was obtained by averaging over number of elements. However, in single element system, it was achieved by averaging over number of sensor rotations. The appropriate weight of the subbands compound was adaptively determined based on the variance-covariance matrix and common for all angle of rotations. The final image of this method for each angle of rotations after feeding back to previous tensor-X is Y_{MVDR} as shown in the figure.

Currently super resolution method SCM was applied to sensor array system with a standard beamforming method for constructing the image. Detail of procedures to apply SCM can be studied

Preprints (www.preprints.org) | NOT PEER-REVIEWED | Posted: 7 December 2023 doi:10.20944/preprints202312.0532.v1

in Appendix-B. In this study, SCM was adaptively applied to single element. However, the SCM application basen on single element system in previous our study was modified by applying compression process to matrix-D resulting the equation $D^H y = D^H D x$. Hence, the SCM profile was computed based on the modified model and multiplied by MVDR output, Y_{MVDR}. The simple averaging or coherence factor (CF) to compound over number of rotations was applied to generate a final image.

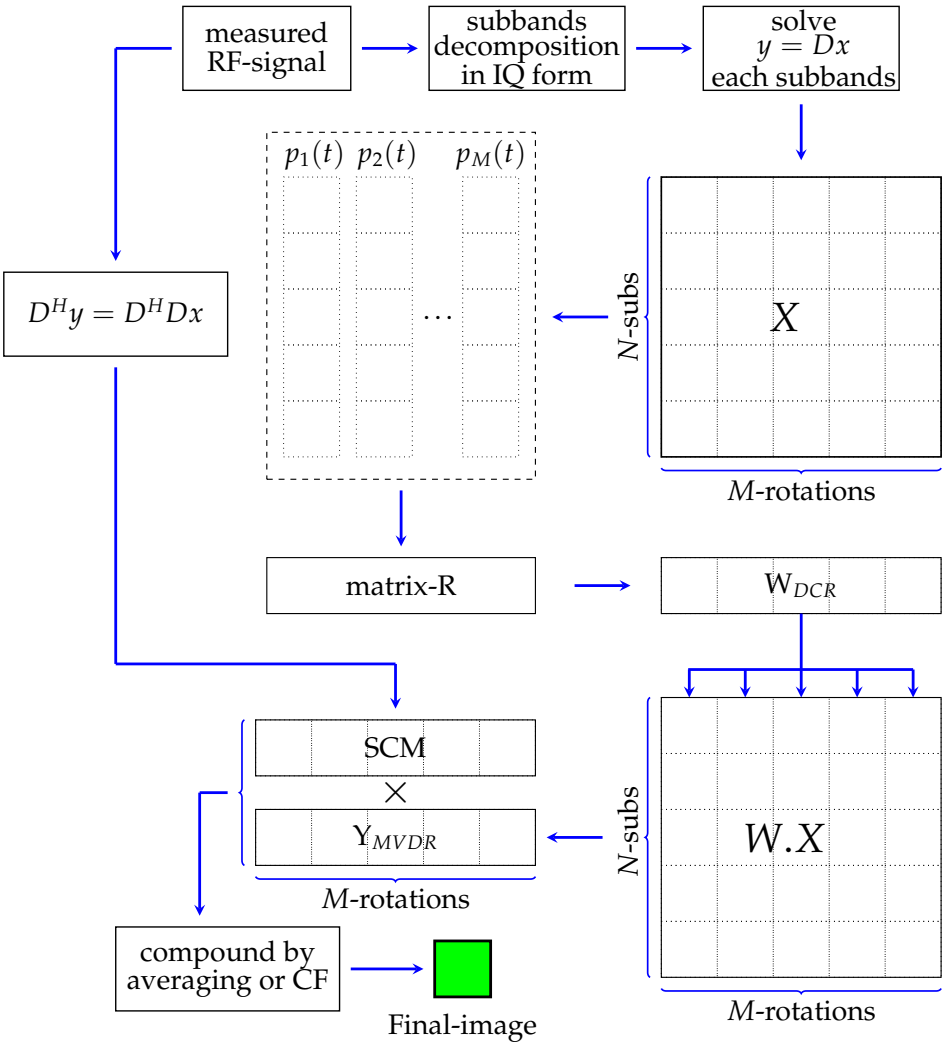

Figure 1. Propose method by integrating the weighted frequency subbands compound and super resolution method (SCM).

properly

2.3. Previous methods for constructing image based on single transducer

In this simulation, several methods was performed to evaluate the image quality and compared to proposed method above. Detail of these will be explained as follows:

- Method-A: In this method, the image was constructed by solving numerically the linear equation (LE) of the image model, $y = Dx$, for each angle of rotations.
- Method-B: This method uses weighted frequency subbands compound to obtain image for each rotation. The original wide band of measured signal was decomposed into several narrow subbands with its different center of frequency. The subband decomposition was applied to vector-y and matrix-D for all angles of rotation. The images were constructed by numerically

 doi:10.20944/preprints202312.0532.v1

solving a linear equation of the image model with different subbands and angles of rotation. By mean-variance distortion-free response (MVDR) method, the weight of each subband was calculated and summed up for each angle of rotation.

- Method-C: Based on image model, $y = Dx$, the SCM profile was extracted from the measured data for each angle of rotation. Th final image at different angle of rotations was obtained by multiplying the SCM profile with image-x computed by numerically solving LE.
- Method-D: The image model was modified by applying the D-compression to the original image model resulting $D^H y = D^H Dx$. The SCM profile was computed based on the modified image model. On the other hand, the solution-x of this equation was computed by solving analytically $x = (D^H D)^{-1} D^H y$. The final image each rotation was achieved by multiplying the image-x and SCM-profile properly.

The final image to compound over number of rotations obtained was applied for all methods by simple averaging or coherence factor (CF).

3. Simulation and Results

3.1. Simulation model

The proposed model was developed using a finite element method (FEM) OnScale, which is a simulator for ultrasound propagation and piezoelectric analysis. Figures 2a-b show the simulation model, which consists of a backing layer, a single PZT element, and an encoding mask with different scatterer number positions using water as the medium for propagating the ultrasonic wave. In reality, a physical device is a circular disk transducer that can be implemented to generate 3D images. However, due to the complexity of the computational process, a 2D simulation was performed in this study. Table 1 shows details of the physical parameters used in the simulation.

The important part of the device is a coding mask attached on the surface of transducer as shown in Figure 2c. It is consisting of number patches with same width. However, the height of each patches are different with a randomized thicknesses with a minimum thickness of 0.25λ and a maximum thickness of 1λ that creating a different local waves propagation with different time delay. The coding mask has a function to generate a spatial coding and a focusing transmitted waveform exceeding from transducer was broken. In this simulation, the transducer was fired by a short pulse with center of frequency (7 MHz) (see Figure 3). The snapshot of FEM simulation in Figures 2 c-d shows clearly the coding mask affects to the transmitted wave outspreading.

Table 1. Physical parameter used in simulation.

Parameter	Value
short transmission pulse voltage	50 Volts
device length	5 mm
center of frequency	7 MHz
backing thickness	1.25 mm
PZT transducer:	
- thickness	0.165 mm
- density	7,500 kg/m^3
- dielectric constant	1,700
coding mask:	
- material	plastic
- density	1060 kg/m^3
- bulk velocity	2,340 m/s
- number of patches	30
- randomized thickness	0.083mm-0.335mm / (0.25λ-1.00λ)
scatterer radius	0.1 mm
distance scatterer to surface of transducer	2.5 mm
region of interest (ROI) size	2 mm$\times$2 mm

Preprints (www.preprints.org) | NOT PEER-REVIEWED | Posted: 7 December 2023 doi:10.20944/preprints202312.0532.v1

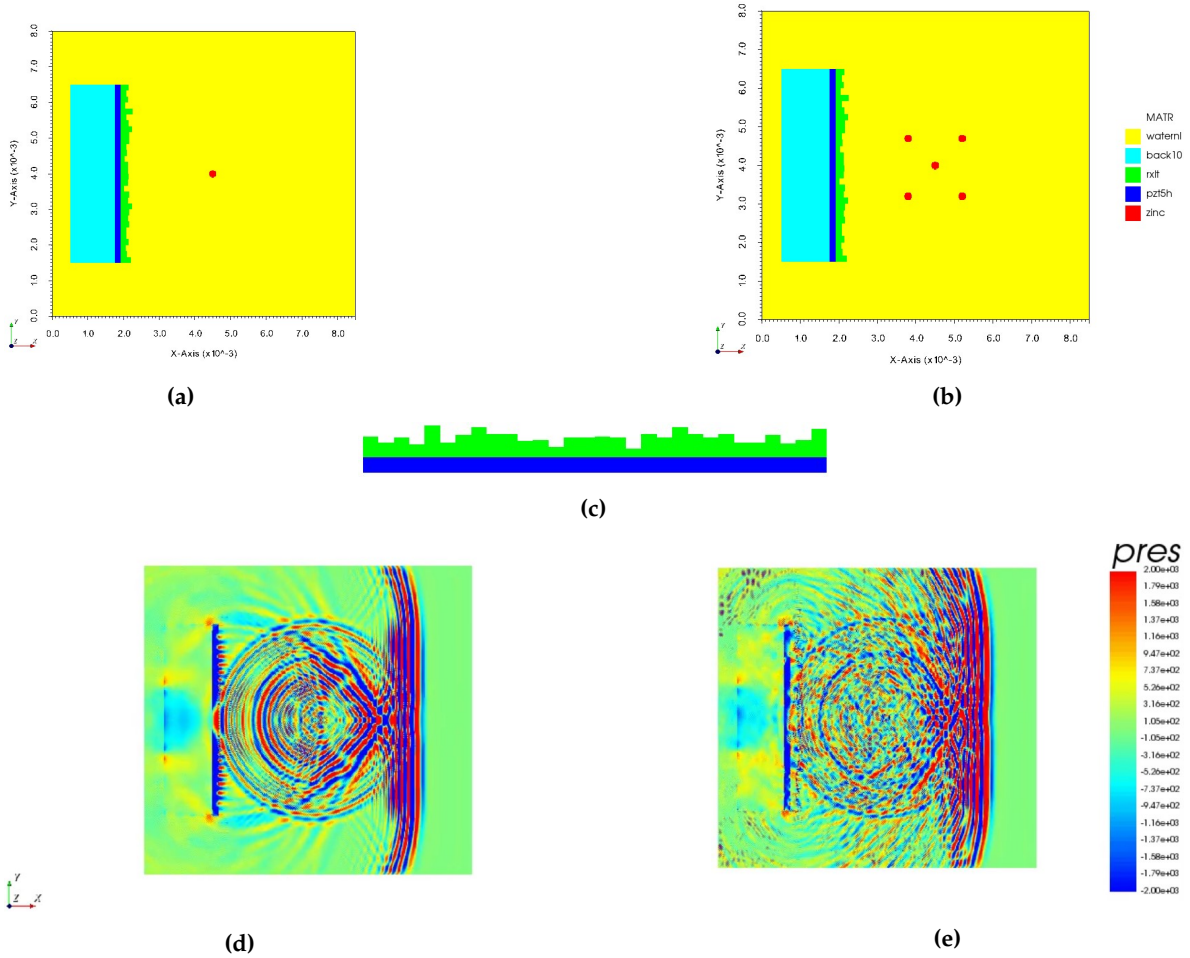

Figure 2. Proposed simulation model with **a**) single scatterer, **b**) multiple scatterers, (**c**) side view of coding mask attached on the top of transducer, screenshot of FEM simulation (**d**) without coding mask and (**e**) with coding mask of single scatterer.

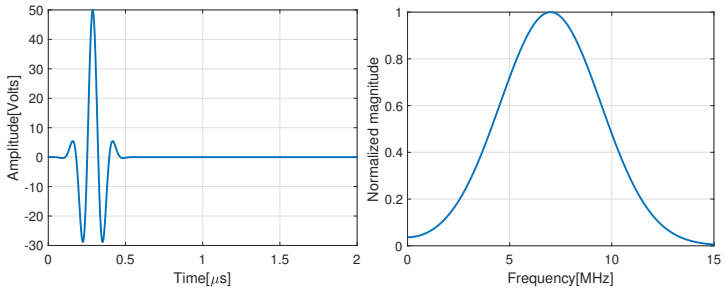

Figure 3. (**a**) Short pulse transmission waveform and (**b**) its center of frequency at 7MHz.

To construct the image due to the model equation, the reflected signal from the scatterers placed in imaging region represented by vector-y and the grid reflected signal at the target region of the matrix-D were measured. The transducer was rotated at 25-angles of rotation for enlarging number of the measurements and enhancing the image resolution. The reflection signal of D at the grid position in the ROI was calculated as follows. First, the sound field in the ROI produced by pulse transmission was calculated. The ROI for the imaging area was set by 2 mm $\times$ 2 mm. A one-sided acoustic transfer function was calculated from the sound pressure waveforms obtained at each point in the ROI and the transmitted pulse. This was then multiplied by the sound pressure waveform at each point to obtain the reflected signal.

Preprints (www.preprints.org) | NOT PEER-REVIEWED | Posted: 7 December 2023 doi:10.20944/preprints202312.0532.v1

3.2. Simulation Result

In this subsection, the simulation results will be presented based on the proposed methods. After performing the model simulation and measuring data required for solving the image model, the post processing and constructed image were performed by MATLAB R2022a. Currently, the image target which is vector-x was obtained by solving numerically Equation (1) using a least squares method (LSQR), that available on the MATLAB library, with setting a iteration residual of 0.1 in this simulation.

3.2.1. Basic method: solving numerically a linear equation of image model

In the previous ultrasound wave simulation, the data consisting of vector y and matrix D were collected at different angles of rotation. The RF signal was converted into an analytical signal (IQ) before solving the linear equation (LE). In this method, the image-x was constructed by numerically solving the image model for each angle of rotation. The image with single scatterer at dept of about 4.5 mm was constructed by different number of angles to evaluate the effect on the image quality as shown in Figure 4a-b-c. In this simulation, two scenarios were applied to compound over the number of rotations. The images on the upside were constructed by simple averaging over the number of rotations. While the bottom images were constructed by applying the coherence factor (CF). The images with CF show the better speckle suppression compared to the simple averaging method. At present, image with 25 rotations shows a better image resolution and a good suppression of unwanted signal. However, the image with 15 rotations does not look much different compared to 25 rotations. To confirm this result, the signal intensity distribution crossing the line through the scatterer position in the range and lateral direction of the CF image was also plotted as shown in Figure 4d-e.

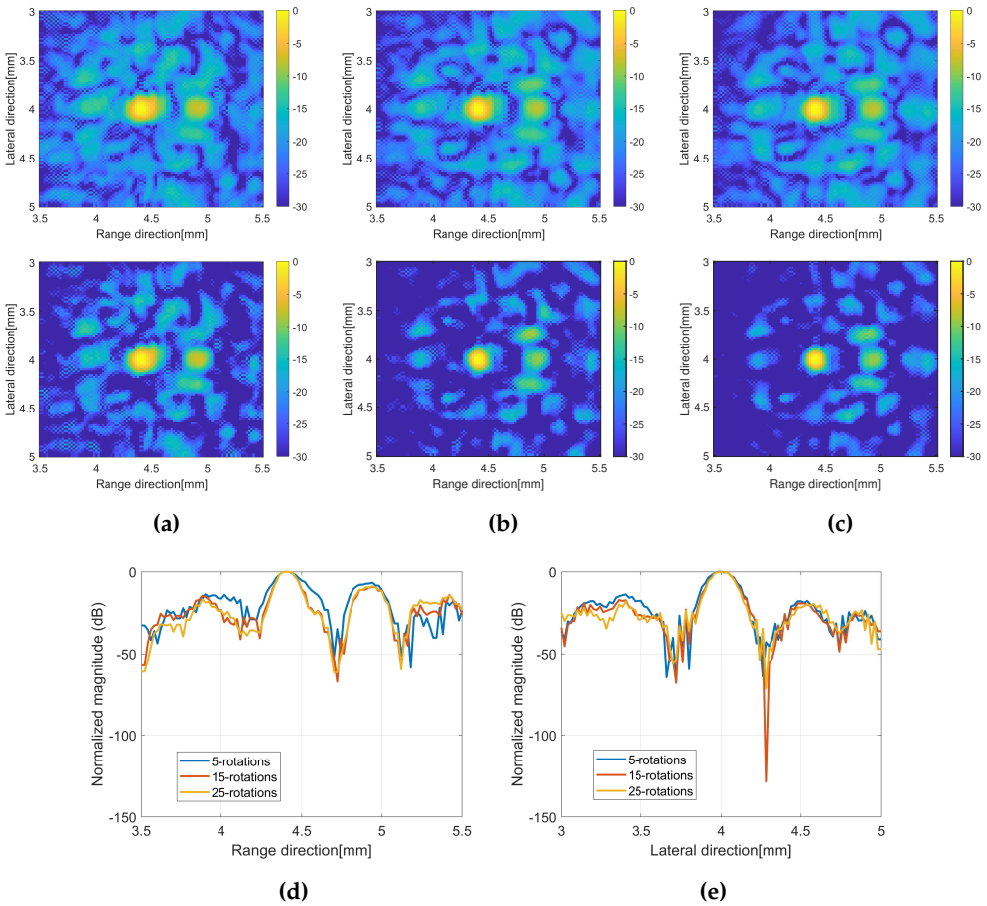

Figure 4. B-mode images constructed by numerically solving the linear equation (LE) with different number of rotations, simple averaging (top) and CF composite (bottom); (**a**) 5-rotations, (**b**) 15-rotations, and (**c**) 25-rotations. Amplitude profile crossing the scatterer position in (**d**) range and (**e**) lateral direction.

Preprints (www.preprints.org) | NOT PEER-REVIEWED | Posted: 7 December 2023 doi:10.20944/preprints202312.0532.v1

3.2.2. Frequency subbands compound

In this method, the original baseband echo was decomposed into 35 subbands with a bandwidth of 6 MHz. Some decomposed subband signals after applying a Hanning window filter can be seen in Figure 5. It shows that the center frequency of the base band (7 MHz) has been changed to a specific frequency for each subband. The decomposition process was performed for the vector y and the matrix D for all rotation angles. The image model for each subband and rotation angle was solved numerically, resulting in 35×25 images. Figure 6 shows the performance of B-mode images in different subbands at the same rotation angle. The image in sub-25 and sub-35 show poor quality due to their sub far from the original center of frequency. The image quality for each subband shows a poor resolution and therefore the subband merging must be performed to improve it.

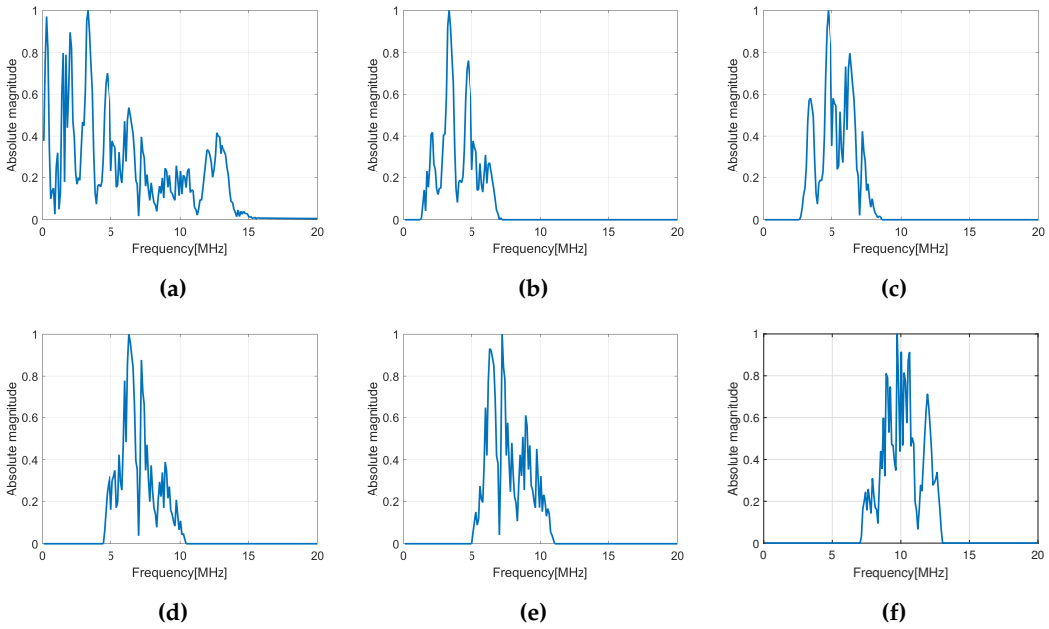

Figure 5. Subband decomposition of a wideband base signal (**a**) into several narrow subband signals in (**b**) to (**f**).

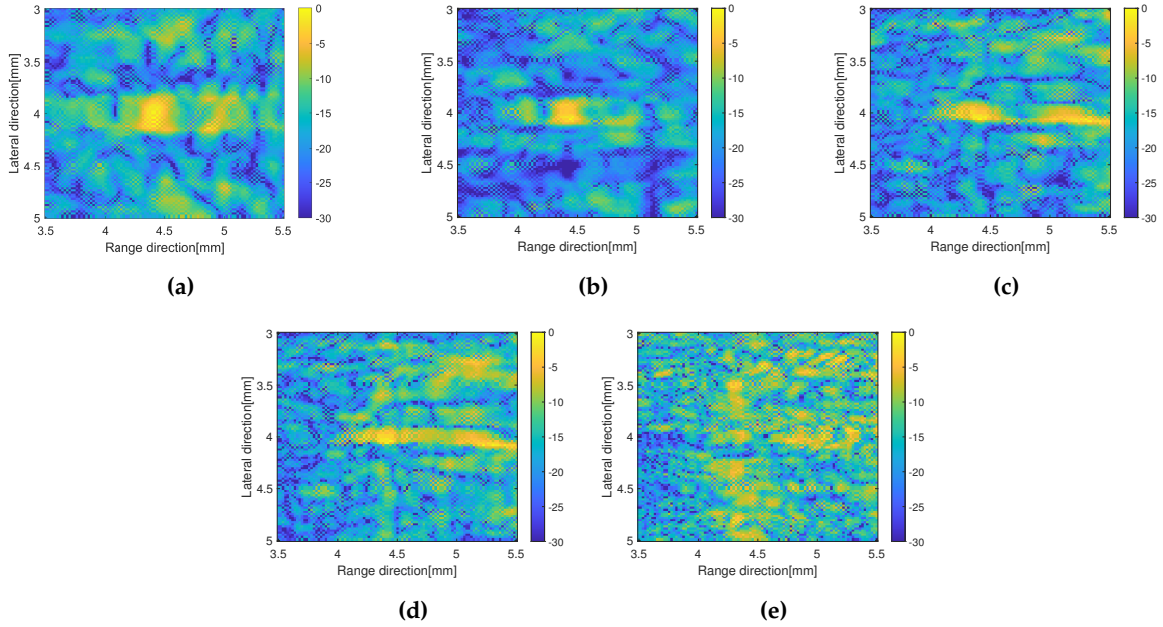

Figure 6. B modes on different subbands with the same rotation angle; (**a**) sub-1, (**b**) sub-8, (**c**) sub-17, (**d**) sub-25, (**e**) sub-35.

Preprints (www.preprints.org) | NOT PEER-REVIEWED | Posted: 7 December 2023 doi:10.20944/preprints202312.0532.v1

In this method, to compound over the number of subbands, we proposed two methods which are simple averaging subbands and weighted frequency subband compound. In the simple averaging method, the image with 35 subbands was averaged for each rotation angle. While in a weighted frequency subband compound, the weight for subbands was calculated and summed up to obtain the image for each rotation angle. The final image was obtained by simple averaging or CF to compound over the number of rotations as in the previous method. Figure 7 shows the B-mode image by simple averaging over the number of subbands and applying weighted frequency subband compounding. The B-mode image by averaging over the number of subbands has better resolution in the range direction compared to the image without subband processing. However, the unwanted signal in the background image is almost the same as before. The image with the CF method is not much different with simple averaging, although it has a better image resolution in the range direction.

The image constructed by a weighted frequency subband average shows a better image quality. By simply averaging the compound over the number of rotations, the image resolution in the range direction was improved. It also suppressed more speckle compared to the averaging subbands method. The image quality became better when the CF method was used to average the image at different angles of rotation. The effect of increasing the number of rotations also affected the image quality as shown in Figure 8 with simple averaging for rotation compounding. The image with 5 rotations shows the poor resolution compared to other images. The images with 15 rotations and 25 rotations are not much different to suppress the unwanted signal. In general, the image by weighted frequency subband combination shows a better image resolution especially in the range direction and has a better speckle suppression.

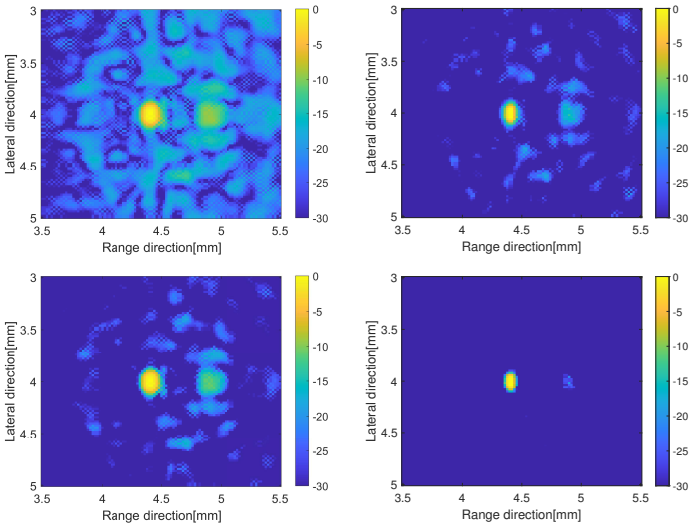

Figure 7. B-mode images by applying the frequency subbands compound, simple averaging (up) and CF compound (down); **a**) averaged subbands and (**b**) weighted frequency subbands compound.

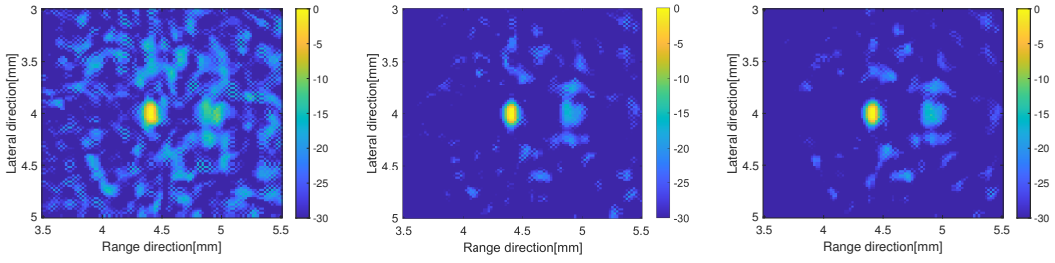

Figure 8. B-mode images by weighted frequency subband method with simple averaging for (**a**) 5-rotations, (**b**) 15-rotations, and (**c**) 25-rotations.

Preprints (www.preprints.org) | NOT PEER-REVIEWED | Posted: 7 December 2023 doi:10.20944/preprints202312.0532.v1

3.2.3. Super-resolution method (SCM)

In previous our study, a super-resolution method (SCM), which was applied to a sensor array system with a chirp transmitted waveform signal and employed a famous beamforming technique to construct the image. It is effective to improve the image resolution by an eigenvalue analysis approach. In this study, the method was adaptively implemented on a single-element system with a short-pulse transmitted waveform signal, and the image was constructed based on a linear equation (LE) of the model.

The SCM was applied to the original image model, $y = Dx$, for all rotation angles. A variance-covariance matrix was first determined by decomposing the echo signal (y) into 35 subbands with a bandwidth of 6 MHz. The eigenvalue and eigenvector were extracted from the matrix for eigenvalue analysis, and the eigenvalue was sorted in descending order to detect the signal and noise subspaces. Figure 9 shows the eigenvalue analysis by extracting an eigenvalue profile. From the profile, the eigenvector corresponding to the first eigenvector with a higher value spans a signal subspace. While the eigenvectors corresponding to the next eigenvalues consist of a noise subspace. By assigning each column of the matrix D in the image model ($y = Dx$) as a steering vector, the noise for each grid position was evaluated for 25 rotation angles, resulting in an SCM profile. The final image was obtained by multiplying the profile with the previously numerically solved image.

To avoid the numerically computation of image-x, the original image model was modified by applying the compression process to matrix-D resulting

$$D^H y = D^H D x,$$
$$y' = Ex, \tag{2}$$

where $y' = D^H y$ and $E = D^H D$. Based on equation 2, the SCM profile was computed for all angles of rotation as the previous strategy. Figures 10a-b show the SCM profile at a given angle of rotation with different approximations. In the case of a single scatterer, the C value was set to 1 to compute the SCM profile. The varying C value affected the SCM profile with the appearance of an unwanted signal as shown in Figure 10c. The SCM profile was plotted in the range direction in a line crossing the scatterer position. B-mode images of a single scatterer (C=1) are shown in Figure 11 with simple averaging and CF composite.

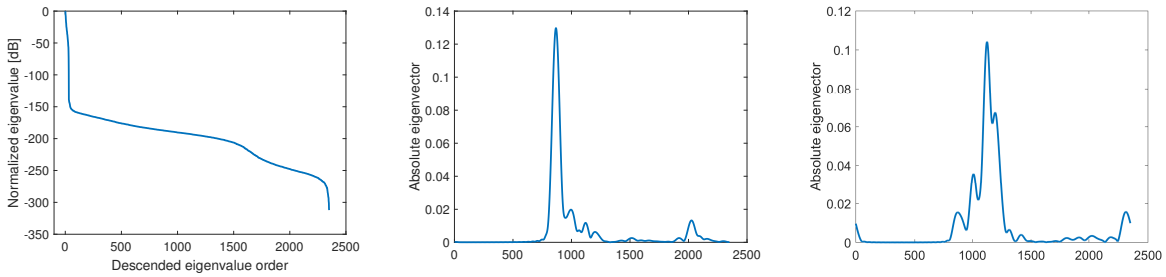

(a) **(b)** **(c)**

Figure 9. Eigenvalue analysis; (**a**) eigenvalue distribution in descend order with (**b**) the first eigenvector and (**c**) second eigenvector corresponding to their eigenvalue respectively.

Preprints (www.preprints.org) | NOT PEER-REVIEWED | Posted: 7 December 2023 doi:10.20944/preprints202312.0532.v1

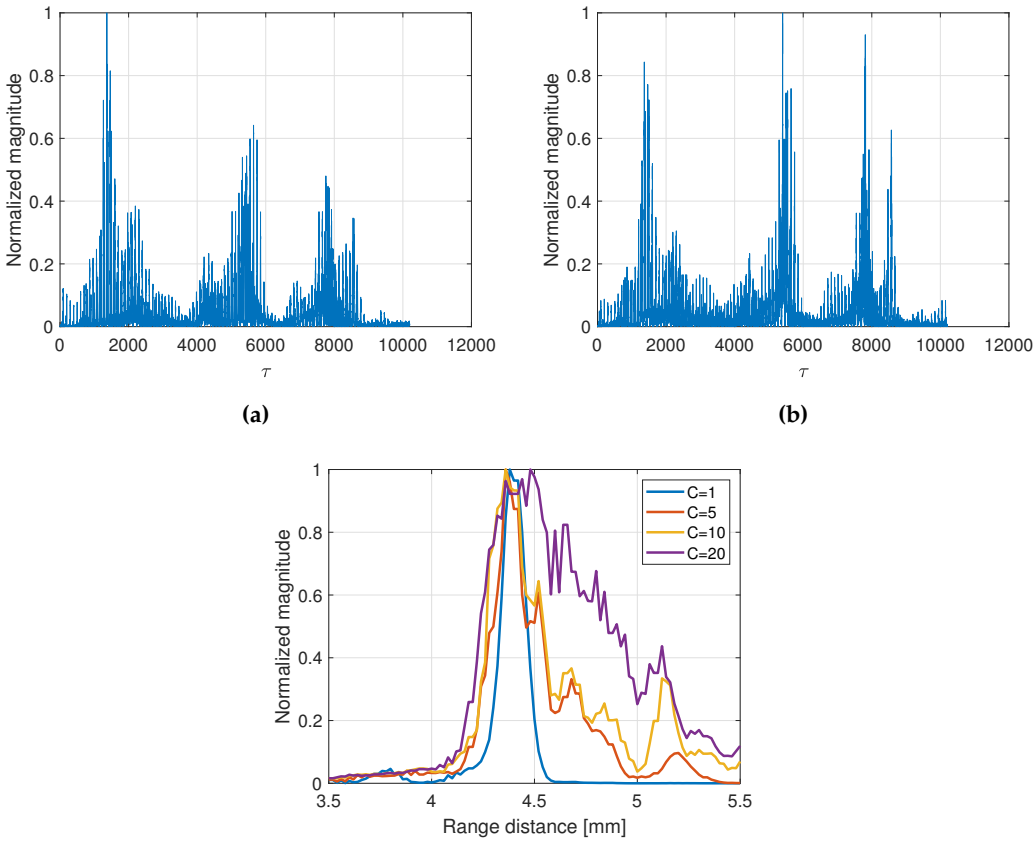

Figure 10. SCM profile (**a**) without compression and (**b**) with *D*-compression process. Effect of different *C*-value to (**c**) SCM profile in range direction.

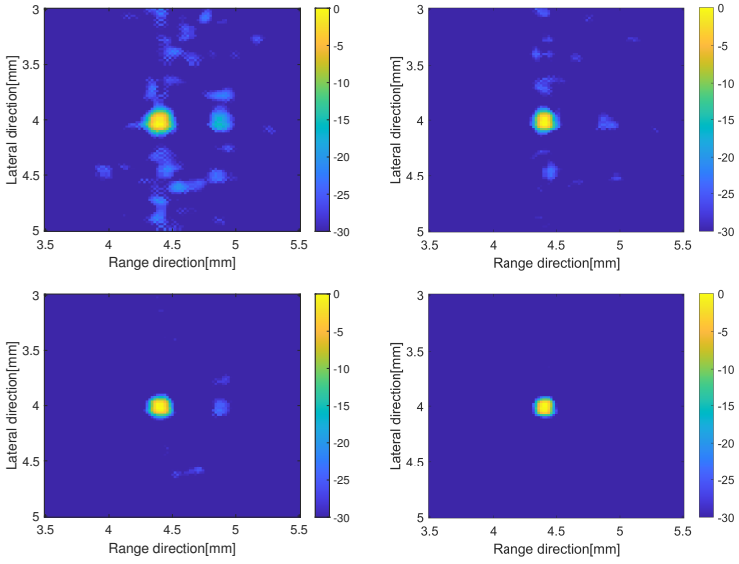

Figure 11. B-mode images by applying super resolution method, simple averaging (up) and CF compound (down), (**a**) no-compression; (**b**) with compression process.

Preprints (www.preprints.org) | NOT PEER-REVIEWED | Posted: 7 December 2023 doi:10.20944/preprints202312.0532.v1

3.2.4. Proposed method

From the presented results before, the image constructed by applying weighted subbands frequency compound has better resolution in range direction only. While by applying a super-resolution method, the image quality has better improvement in lateral direction. In current super-resolution method, the image was obtained by multiplying the image x by the computed SCM profile for each angle of rotations. Therefore, we integrated both methods for obtaining better image quality as our proposed method. The SCM profile was multiplied by the image obtained by applying weighted frequency subbands method. Figure 12 shows B-mode images with simple averaging and CF compound respectively. To provide the qualitative performance of the explained methods, Figure 13 shows the amplitude profiles in range and lateral resolution. The cross-sectional profile was obtained by picking up a normalized intensity along the line passing through the target position in range and lateral direction of the image with CF compound.

To investigate the effectiveness of the methods, the single scatterer was placing at Different scatterer positions were performed and evaluated. A single target with the same properties and size was placed at nine positions in the imaging region. Three parameters were used to evaluate the image characteristics: signal-to-noise ratio (SNR), speckle level, and full width at half maximum (FWHM). SNR in dB was calculated by dividing the averaged signal by the standard deviation of the noise. Speckle level in dB was determined by averaging the image noise. FWHM was calculated at -3 dB of the amplitude profile intersecting the single scatterer of the image with CF compound. Figure 14 shows signal to noise ratio (SNR), speckle level and full width at half magnitude (FWHM).

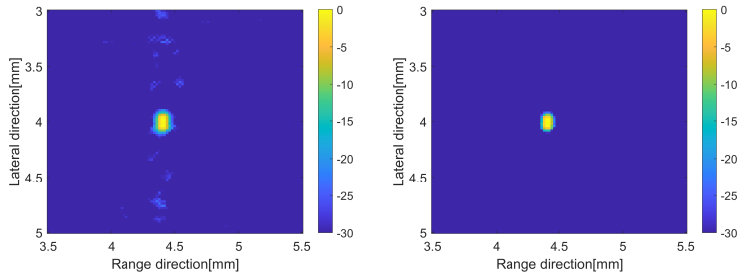

(a) **(b)**

Figure 12. B-mode images by integrating weighted frequency subbands and SCM with (**a**) simple averaging; (**b**) CF compound.

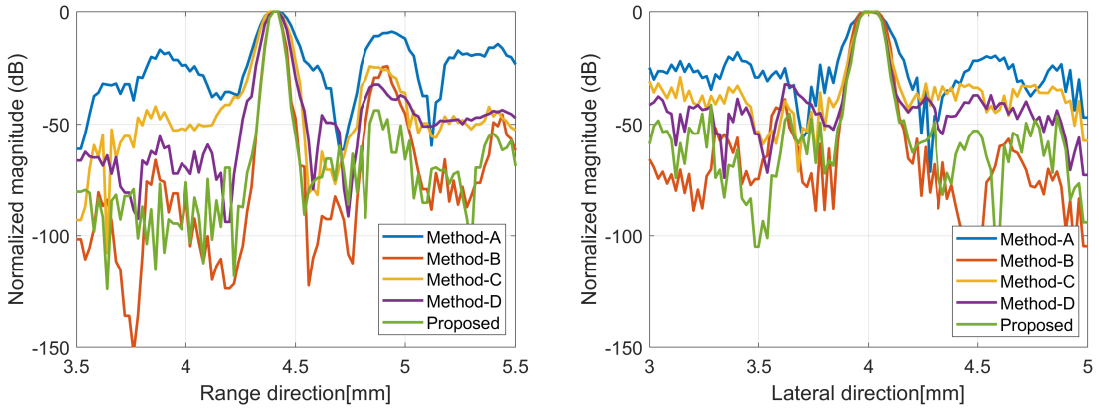

(a) **(b)**

Figure 13. Amplitude profile of B-mode image of CF compound at (**a**) range and (**b**) lateral direction.

Preprints (www.preprints.org) | NOT PEER-REVIEWED | Posted: 7 December 2023 doi:10.20944/preprints202312.0532.v1

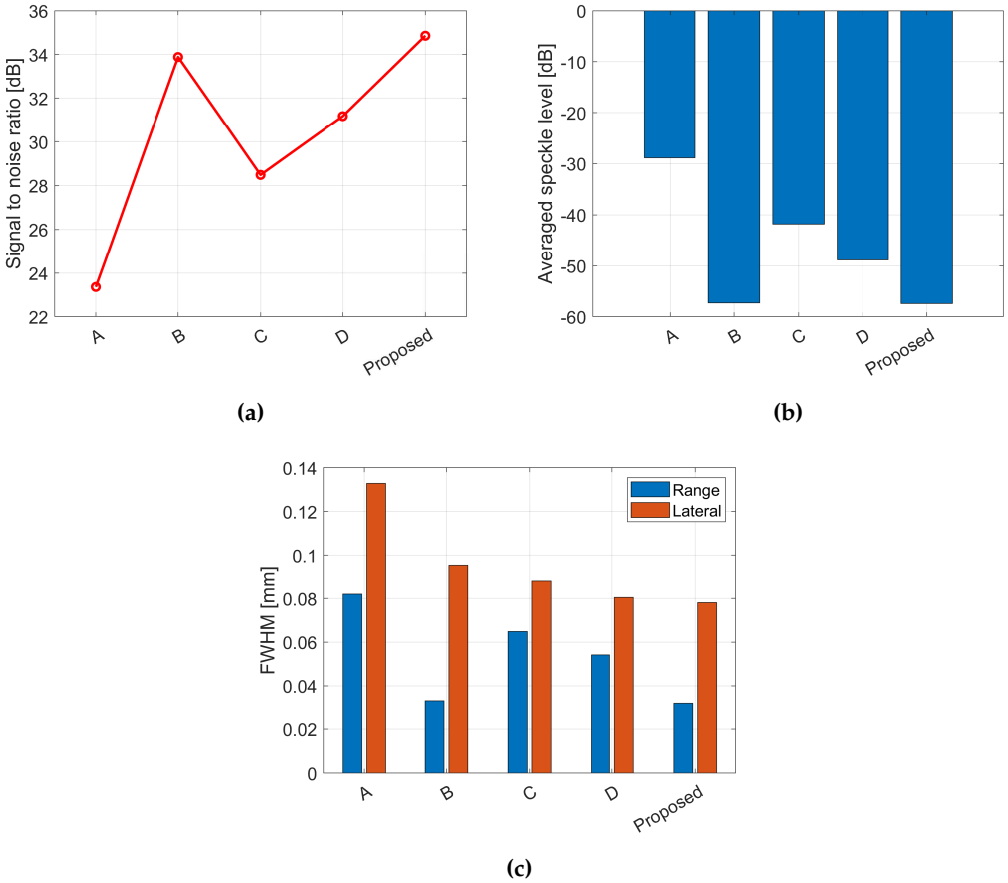

Figure 14. (**a**) Signal to noise ratio (SNR); (**b**) speckle level; (**c**) FWHM.

3.2.5. Evaluate the methods with multiple scatterers

Instead of single scatterers, we also investigate the imaging characteristic by placing multiple targets (5-scatterers) in front of device. The target has same properties and size as the imaging with single scatterer before. To compute SCM profile, for 5-scatterers, C-value in Equation A15 was set to be 5. The Figure 15 shows the B-mode images with different methods applied for multiple scattererers. The image with integrating between weighted frequency subbands compound and SCM with compression shows better resolution.

Preprints (www.preprints.org) | NOT PEER-REVIEWED | Posted: 7 December 2023 doi:10.20944/preprints202312.0532.v1

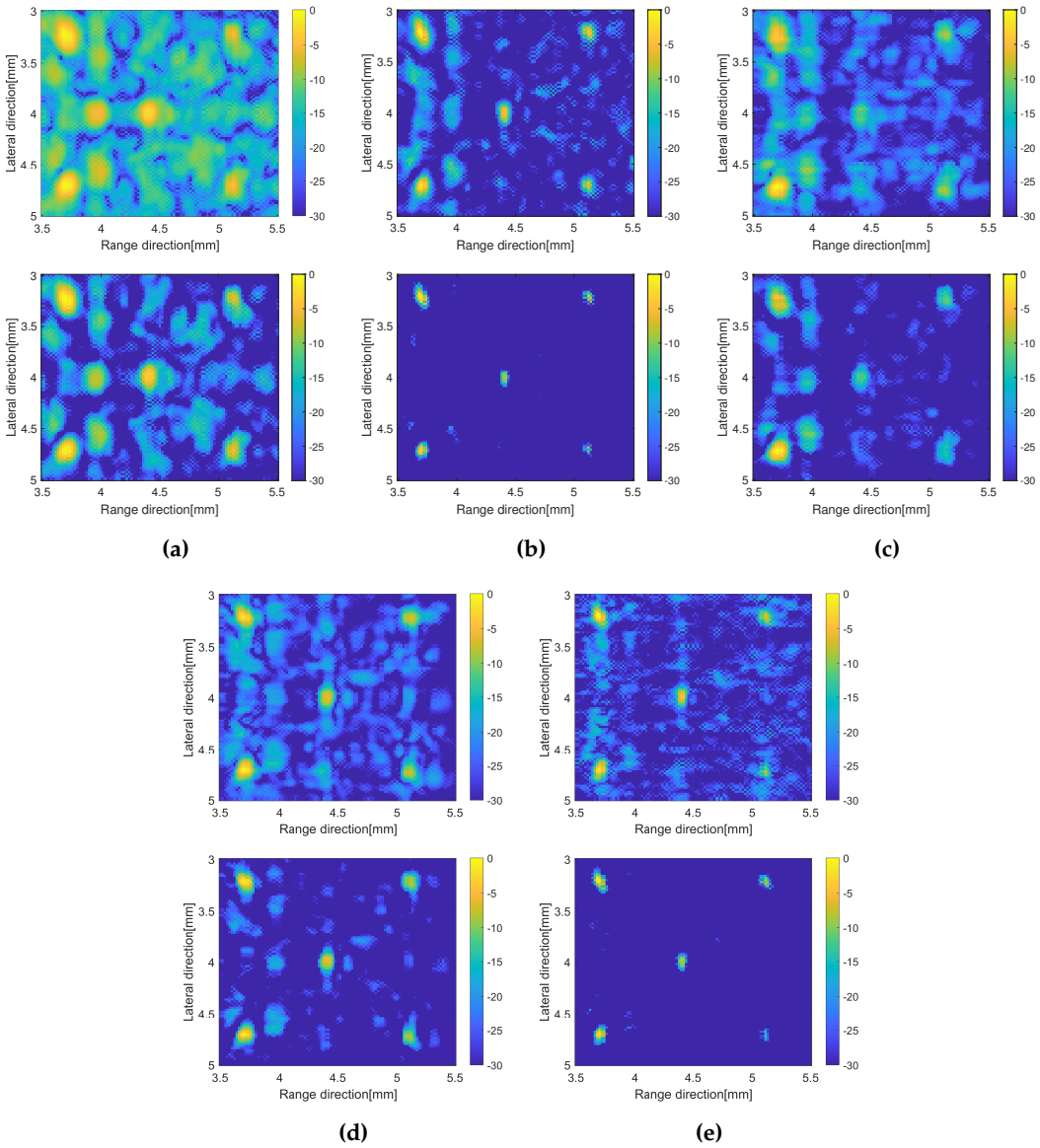

Figure 15. B-mode images with multiple scatterers with simple averaging (up) and CF compund (down), (**a**) solving the original LE, (**b**) weighted frequency subbands compound; (**c**) apply super resolution method; (**d**) apply super resolution method with compression; (**e**) integrate weighted frequency subbands and super resolution with compression.

4. Discussion

The original image, which is constructed by solving the linear equation at each angle of rotation without any processing, has been improved. The weighted frequency subband composite shows the best image resolution in the range direction and higher speckle suppression compared to other methods. To achieve better spatial coding, the number of measurements in the single-element system was increased by increasing the number of rotations. Speckle suppression and spatial resolution improved as the number of rotations increased, as shown in Figure 8 with simple averaging.

In range direction resolution, the image carried out by applying the SCM has been effectively work. The C value is set depending on the number of scatterers. The noise is included when the C value is higher, as shown in Figure 10c. Figure 11 confirms the effect of D compression, which effectively improved the image resolution in both directions compared to the SCM without compression. It also provided better speckle suppression performance. Therefore, we integrated both methods to achieve

Preprints (www.preprints.org) | NOT PEER-REVIEWED | Posted: 7 December 2023 doi:10.20944/preprints202312.0532.v1

better image quality. The quantitative evaluation of the image performance of single element system with few methods shown in Figure 14.

The proposed methods also shows the better image quality when applied to multiple targets as shown in Figure 15. By simple averaging to compound over number of rotations, the integrated method between weighted frequency subbands compound and super resolution methods shows the better image resolution.

5. Conclusions

In this study, the ultrasonic imaging of an encoding mask based on a single oscillator has been successively constructed. The imaging resolution has been evaluated by using several methods, which are weighted frequency subband connections, super resolution method (SCM), and integration of both methods as our proposed method in this study. The simple averaging and the coherence factor (CF) were applied for composing the final image over 25 angles of rotation. In the range direction, the best resolution image was demonstrated by weighted subband frequency summation. While the lateral resolution was demonstrated by a super-resolution method. Our proposed method by combining weighted subband frequency compounding and super-resolution technique shows the best image quality. The evaluation was done by calculating the FWHM, SNR and speckle level of the image. In the future, the experimental stage will be conducted to confirm the current simulation results.

Author Contributions: Authors contributed as follows: performed the simulation and experiment: M.S. and E. N.; provided overall guidance: N.T.; provided other support: M.Y.

Funding: This research received no external funding.

Conflicts of Interest: The authors declare no conflict of interest.

Appendix A. Frequency subband compound

Frequency compounding is a common method for improving the resolution of ultrasound images. The original wide-band of measured IQ signal at different angles was subdivided into M narrow subbands as shown in Figure A1. By using Equation 1, vector-x for each subbands for all angles of ratotations was computed resulting the following tensor data $\mathbf{X}$,

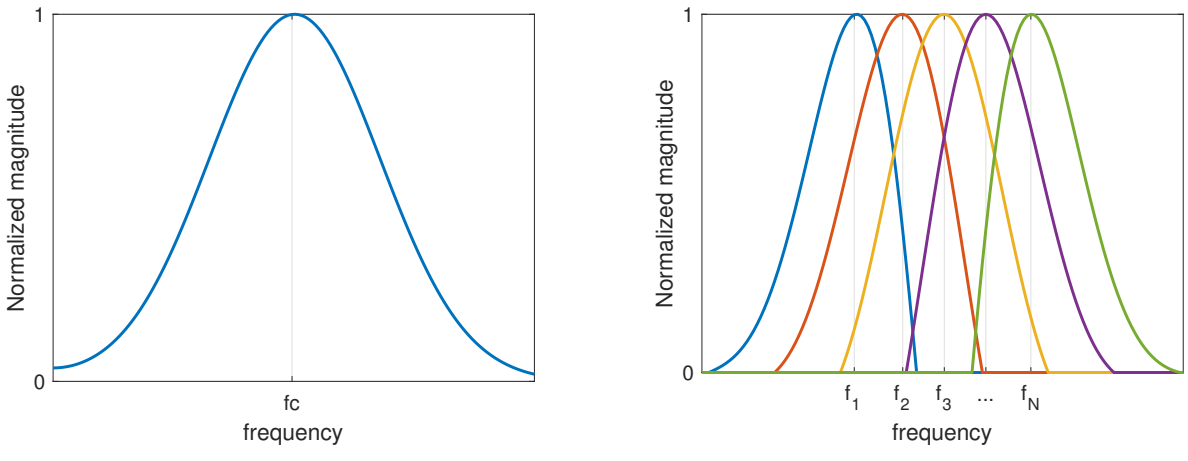

Figure A1. Subbands compound; (**a**) original band with f_c as a center of frequency; (**b**) extracted subbands with a different center of frequency.

Preprints (www.preprints.org) | NOT PEER-REVIEWED | Posted: 7 December 2023 doi:10.20944/preprints202312.0532.v1

$$\mathbf{X} = \begin{bmatrix} x_{1,1} & x_{1,2} & \dots & x_{1,N} \\ x_{2,1} & x_{2,2} & \dots & x_{2,N} \\ \vdots & \vdots & \ddots & \vdots \\ x_{M,1} & x_{M,2} & \dots & x_{M,N} \end{bmatrix} \tag{A1}$$

where $x_{i,j}$ denotes the pixel value at subband-i and angle-j. Following to [21] the frequency subbands compound is started by computing the variance covariance matrix-R that requires the following vector s_j,

$$s_j = \frac{1}{N-1} \sum_{l=1, l \neq j}^{N} (x_{ij})_l, \tag{A2}$$

and matrix R is given by

$$R = \frac{1}{N} \sum_{j=1}^{N} s_j s_j^H + \epsilon I, \tag{A3}$$

where H indicates Hermitian transpose, ϵ is diagonal loading parameter, and I represents an identify matrix. The number of rotation angles N is required for averaging matrix-R as well as for averaging the frequency sub-bands. The weight of frequency compound each angle is determined by

$$w_j^F = \frac{R^{-1} 1_L}{1_L^\intercal R^{-1} 1_L}, 1_L = [1, \dots, 1]^\intercal. \tag{A4}$$

The frequency contraction is computed by:

$$y_j = \frac{1}{M} \sum_{i=1}^{M} (w_j^F)^H (x_{ij}). \tag{A5}$$

This process is applied to all grids corresponding to the pixels of the ROI. Equation (A5) is computed for all angles of rotations for each grid. To compound over number of angles, the average and coherence factor (CF) are used as the final value for each grid. The magnitude of the complex number is then the image luminance value.

Appendix B. Super-resolution method (SCM)

Multiple echo signals $y(t)$ from scatterers are received with transmitting signal $s(t)$. It is expressed in term of the convolution of the transmitted signal and impulse response $h(t)$ of the channel as

$$y(t) = \int_{-\infty}^{\infty} h(\tau) u(t-\tau) d\tau. \tag{A6}$$

By assuming the received echo signals compress number of echo signals from C-scatterers with different delay times, hence an impulse response $h(t)$ is defined by

$$h(t) = \sum_{i=l}^{C} h_i \delta(t - \tau_i), \tag{A7}$$

where h_i is a set of complex amplitudes, τ_i represents a set of propagation delay times to be estimated and $\delta(\cdot)$ is the Dirac delta function.

Considering multipath propagation, the correlator output $z(\zeta)$ is the superposition of scaled copies of the chirp signals auto correlation. The cross-correlation of echo with transmission signal $s(t)$ is

Preprints (www.preprints.org) | NOT PEER-REVIEWED | Posted: 7 December 2023 doi:10.20944/preprints202312.0532.v1

$$v(\zeta) = \sum_{i=l}^{C} h_i r(\zeta - \tau_i) + \eta(\zeta). \tag{A8}$$

Therein, $r(\zeta)$ is the auto-correlation function of the chirp signal and $\eta(\zeta)$ is the cross correlation of the chirp signal and the noise process $\eta(\zeta)$. The received signal $z(\zeta)$ is described in the base band as follows

$$z(\zeta) = \sum_{i=l}^{C} h_i e^{-j\omega_0\tau_i} r(\zeta - \tau_i) + \mu(\zeta). \tag{A9}$$

Next, a delay profile vector is defined by $z(\zeta) = [z(\zeta_1)z(\zeta_2)\cdots z(\zeta_M)]^T$. With steering vector $r(\tau_i) = [r(\zeta_1 - \tau_i)r(\zeta_2 - \tau_i)\cdots r(\zeta_M - \tau_i)]^T$, thus $z(\zeta)$ might expressed as

$$z(\zeta) = \sum_{i=l}^{C} h_i e^{-j\omega_0\tau_i} r(\tau_i) + \mu. \tag{A10}$$

The steering vector $r(\tau)$ might calculated for any τ since the auto-correlation function $r(\cdot)$ is known. In terms of the array manifold matrix $\Gamma = [r(\tau_1)r(\tau_2)\cdots r(\tau_C)]^T$ and the gain vector, $g = [h_1 e^{-j\omega_0\tau_1} h_2 e^{-j\omega_0\tau_2} \cdots h_C e^{-j\omega_0\tau_C}]^T$, the delay profile vector takes the form

$$z = \Gamma g + \mu. \tag{A11}$$

The covariance matrix $R = E\{zz^H\}$ can also be written as

$$R = \sum_{i,j} E\{h_i h_j^*\} e^{-j\omega_0(\tau_j - \tau_i)} r(\tau_i) r(\tau_j)^H + E\{vv^H\}. \tag{A12}$$

The following form of R will be used:

$$R = \Gamma G \Gamma + R_n, \tag{A13}$$

where G is covariance matrix $G = E\{gg^H\}$. The noise correlation matrix R_n can be expressed as $R_n = E\{\mu\mu^H\} = \tau^2 R_0$, where R_0 is a Hermitian matrix whose klth element is $r(\zeta_k - \zeta_l)$. The SCM relies on a generalized eigendecomposition of the following form:

$$Re_i = \lambda_i R_0 e_i : i = 1, 2, \ldots, M, \tag{A14}$$

and the validaty of the following assumption: The number of samples at the correlator output is greater than the number of paths (i.e. $M > C$). Furthermore, the column of Γ are lineraly independent, G is nonsingular. Under this conditions, the signal covariance matrix $R - R_n$ will have rank C, and R will have C generalized eigenvalues greater than σ^2 and $M - C$ generalized eigenvalue equal to σ^2. The set of C eigenvector $\{e_i\}_{i=0}^{C}$ corresponding to the C largest generalized eigenvalues span the signal subspace, and the set of $M - C$ smallest generalized eigenvector $\{e_i\}_{i=C+1}^{M}$ corresponding to the C largest generalized eigenvalues span the noise subspace. It can be shown that the noise subspace is orthogonal to the columns of matrix Γ, i.e., the noise subspace is orthogonal to the steering vectors evaluated at the true delays. In order to estimate the delay, we use a measure of the ortyhoganality of the steering vector to $\{e_i\}_{i=C+1}^{M}$. Accordingly, a super-resolution delay profile $S(\tau)$ based on the MUSIC algorithm might be defined as

$$SCM(\tau) = \frac{r(\tau)^H R_0^{-1} r(\tau)}{\Sigma_{i=C+1}^{M} |r(\tau)^H e_i|^2}. \tag{A15}$$

 doi:10.20944/preprints202312.0532.v1

Appendix C. Coherence factor beamformer

In this study, instead of simple averaging to compound the image over the number of rotation, we used Coherence factor (CF). CF is an effective beamformer for removing the background signal [28]. The CF is defined by the following equation

$$CF = \frac{|\Sigma_{i=1}^{N} x_i|^2}{N\Sigma_{i=1}^{N}|x_i|^2}, \tag{A16}$$

thus,

$$Y_F = CF \times \Sigma_{i=1}^{N} x_i. \tag{A17}$$

References

1. Synnevag, J.F.; Austeng, A.; Holm, S. Adaptive beamforming applied to medical ultrasound imaging. *IEEE Trans. Ultrason. Ferroelectr. Freq. Control* **2007**, *54*, 1606–1613.
2. Hasegawa, H. Improvement of range spatial resolution of medical ultrasound imaging by element-domain signal processing. *Jpn. J. Appl. Phys.* **2017**, *56*, 07JF02.
3. Danilouchkine, M. G.; van Neer, P. L. M. J.; Verweij, M. D.; Matte, G. M.; Vletter, W. B.; van der Steen, A. F. W.; de Jong, N. Single pulse frequency compounding protocol for superharmonic imaging. *Phys. Med. Biol.* **2013**, *58*, 4791–4805.
4. Ishikura, S.; Yoshizawa, M.; Tagawa, N.; Irie, T. Visualization of frequency dependence of tissue characteristics by phase-contrast imaging based on ultrasonic interference method. *Jpn. J. Appl. Phys.* **2018**, *57*, 07LF20.
5. Youn, J.; Luijten, B.; Bo Stuart, M.; Eldar, Y. C.; van Sloun, R. J. G.; Arendt Jensen, J. Deep learning models for fast ultrasound localization microscopy. In Proceedings of the IEEE International Ultrasonics Symposium, Las Vegas, NV, USA, 7-11 September 2020; pp. 1–4.
6. Matrone, G.; Savoia, A. S.; Caliano, G.; Magenes, G. The delay multiply and sum beamforming algorithm in ultrasound B-mode medical imaging. *IEEE Trans. Med. Imaging* **2015**, *34*, 940–949.
7. Sannou, F.; Nagaoka, R.; Hasegawa, H. Estimation of speed of sound using coherence factor and signal-to-noise ratio for improvement of performance of ultrasonic beamformer. *Jpn. J. Appl. Phys.* **2020**, *59*, SKKE14.
8. Camacho, J.; Parrilla, M.; Fritsch, C. Phase coherence imaging. *IEEE Trans. Ultrason. Ferroelectr. Freq. Control* **2009**, *56*, 958–974.
9. Capon, J. High-resolution frequency-wavenumber spectrum analysis. In Proceedings of the IEEE, August 1969; pp. 1408–1418.
10. Asl, B. M.; Mahloojifar, A. A low-complexity adaptive beamformer for ultrasound imaging using structured covariance matrix. *IEEE Trans. Ultrason. Ferroelectr. Freq. Control* **2012**, *59*, 660–667.
11. Irie, T.; Hasegawa, T.; Sato, M; Tagawa, N.; Tanabe, M.; Yoshizawa, M.; Iijima, T.; Moriya, T.; Itoh, K. Transmission of 100-MHz-range ultrasound through a fused quartz fiber. In Proceedings of the IEEE International Ultrasonics Symposium, Dresden, Germany, 7-10 October 2012; pp. 358–361.
12. Irie, T.; Hasegawa, T.; Itoh, K.; Hirota, N.; Tagawa, N.; Yoshizawa, M.; Moriya, T.; Iijima, T. Tissue imaging using the transmission of 100-MHz-range ultrasound through a fused quartz fiber. In Proceedings of the IEEE International Ultrasonics Symposium, Prague, Czech Republic, 21-25 July 2013; pp. 2010–2013.
13. Tanter, M.; Fink, M. Ultrafast imaging in biomedical ultrasound. *IEEE Trans. Ultrason. Ferroelectr. Freq. Control* **2014**, *61*, 102–119.
14. Nguyen, N. Q.; Prager, R. W. A spatial coherence approach to minimum variance beamforming for plane-wave compounding. *IEEE Trans. Ultrason. Ferroelectr. Freq. Control* **2018**, *65*, 522–534.
15. Ni, P.; Lee, H. N. High-resolution ultrasound imaging using random interference. *IEEE Trans. Ultrason. Ferroelectr. Freq. Control* **2020**, *67*, 1785–1799.
16. Sternini, S.; Pau, A.; Di Scalea, F. L. Minimum-variance imaging in plates using guided-wave-mode beamforming. *IEEE Trans. Ultrason. Ferroelectr. Freq. Control* **2019**, *66*, 1906–1919.
17. Janjic, J.; Kruizinga, P.; van der Meulen, P.; Springeling, G.; Mastik, F.; Leus, G.; Bosch, J. G.; van der Steen, A.F.W.; van Soest, G. Structured ultrasound microscopy. *Appl. Phys. Lett.* **2018**, *112*, 251901.

18. Kruizinga, P.; van der Meulen, P.; Fedjajevs, A.; Mastik, F.; Springeling, G.; de Jong, N.; Bosch, J. G.; Leus, G. Compressive 3D ultrasound imaging using a single sensor. *Sci. Adv.* **2017**, *3*, e170142.
19. Kozai, R.; Tagawa, N.; Yoshizawa, M.; Irie, T. Optimization of frequency and plane-wave compounding by minimum variance beamforming. In Proceedings of the IEEE International Ultrasonics Symposium, Las Vegas, NV, USA, 7-11 September 2020; pp. 1–5.
20. Zhu, J.; Tagawa, N. Improvement of performance degradation in synthetic aperture extension of enhanced axial resolution ultrasound imaging based on frequency sweep. *Sensors* **2019**, *19*, 2414.
21. Zheng, J.; Tagawa, N.; Yoshizawa, M.; Irie, T. Plane wave beamforming with adaptively weighted frequency compound using bandpass filtering. *Jpn. J. Appl. Phys.* **2021**, *60*, SDDB08.
22. Saito, Y.; Tagawa, N. One-shot beam-forming with adaptively weighted compound of multiple transmission angles and subbands. *Jpn. J. Appl. Phys.* **2022**, *61*, SG1079.
23. Syaryadhi, M.; Tagawa, N. Applying Frequency Compound to Enhance Image Resolution of Single Integrated Irregular-Lens Oscillator. In Proceedings of the 43th Symposium on UltraSonic Electronics, Kyoto, Japan, 7-9 November 2022; pp. 1–2.
24. Syaryadhi, M.; Tagawa, N.; Yang. M. Weighted frequency subband compounding in ultrasonic imaging sensor consisting of a single transducer and a random coding mask. In Proceedings of the 2023 IEEE Applied Sensing Conference (APSCON), Bangalore, India, 23–25 January 2023; pp. 1–3.
25. Syaryadhi, M.; Zheng, J.; Tagawa, N.; Yang. M. Super-resolution based on frequency dependence of echo phase rotation in 3D ultrasound imaging by spatially encoded transmit/receive. In Proceedings of the 2023 International Congress on Ultrasonics, Beijing, China, 18–21 September 2023; pp. 00–00.
26. Syaryadhi, M.; Nakazawa, E.; Tagawa, N.; Yang, M. Super-resolution ultrasound imaging with a single coding mask transducer. In Proceedings of the 44th Symposium on UltraSonic Electronics, Toyama, Japan, 13-15 November 2023; pp. 1–2.
27. Fujiwara, M.; Okubo, K.; Tagawa, N. Novel technique for high resolution ultrasound super resolution FM-Chirp Correlation Method (SCM). In Proceedings of the IEEE International Ultrasonics Symposium, Rome, Italy, 20–23 September 2009; pp. 2390–2393.
28. Li, P. C.; Li, M. L. Adaptive imaging using the generalized coherence factor. *IEEE Trans. Ultrason. Ferroelectr. Freq. Control* **2003**, *50*, 128–141.